Mechanical Engineering Journal

DOI:10.1299/mej.17-00442

Received date : 31 August, 2017

Accepted date : 9 January, 2018

J-STAGE Advance Publication date : 19 January, 2018

Robust throwing design based on dynamic sensitivity analysis

Masafumi OKADA*, Shota ONIWA** and Wataru HIJIKATA*
* Dept. of Mechanical Engineering, Tokyo Institute of Technology
2-12-1 Oookayama Meguro-ku Tokyo 152-8552, JAPAN
E-mail: okada.m.aa@m.titech.ac.jp
** Dept. of Mechanical and Intelligent Systems Engineering, Tokyo Institute of Technology
2-12-1 Oookayama Meguro-ku Tokyo 152-8552, JAPAN

Abstract
Throwing an object by a powered robotic system is an effective way for object manipulation in long distance. The focus of the throwing is on the accuracy of the landing point with respect to model uncertainties or disturbances. A robust controller is often designed, however, the motion will be finished before the controller produces its effects because throwing is fast and highly dynamic. Moreover, the robot system sometimes has zero adjustment error in the initial position on its joint angle. This error cannot be overcome by a robust controller. So far, we have proposed a dynamic sensitivity analysis method of throwing for a feed-forward controlled manipulator. The sensitivity of the landing point with respect to zero adjustment error has been calculated, and robust throwing with small sensitivity has been designed. In this paper, the conventional method is applied to a feed-forward/back controlled manipulator in the real world, and evaluations are executed by using a prototyped three-link manipulator. The effectiveness of the proposed method is evaluated based on the sensitivity and variance of the landing point, and a robust throwing with small sensitivity is designed.

Keywords : Sensitivity analysis, Throwing motion, Robust motion design, Motion optimization

1. Introduction

Throwing an object by a powered robotic system is an effective way for object manipulation in long distance or unmanned environments. As shown in Fig. 1, throwing a sensor system to gather environmental information in the disaster-stricken area, throwing a wired object for wiring in mountainous region are examples of effective throwing. The

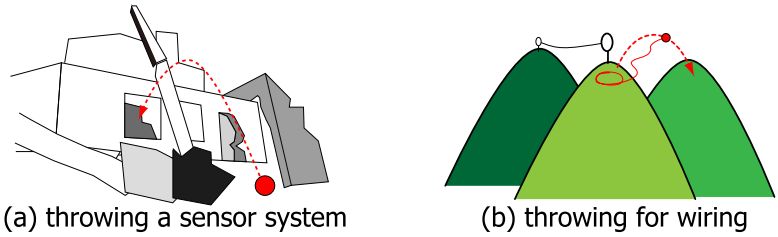

Fig. 1 Application of throwing by a powered manipulator

conventional researches on throwing are mainly divided into mechanism design, control and applications. Tsukakoshi et al. (Tsukakoshi, Watari, Fuchigami and Kitagawa, 2012) developed casting device for search and rescue operation in disaster site. They emphasized the effectiveness of throwing an object to gather information in unmanned area and developed casting system. Fagiolini et al. (Fagiolini, Arisumi and Bicchi, 2011) developed a casting robot that throws its end-effector to catch objects which are far from the robot. Frank et al. (Frank, Barteit and Kupzog, 2008) suggested to use throwing for industrial applications for speed up transportation of parts. The throwing motion was designed by dynamical considerations, and the end-effector was controlled using a vision system. The accuracy of the landing point is one of the

main focuses of throwing. Because of model uncertainties or disturbances, the robot has to be robust controlled. Mason and Lynch defined dynamic manipulation (Mason and Lynch, 1993) as a manipulation with not only kinematics and statics but also dynamic forces, and developed throwing motion controlling under-actuated objects (Lynch and Mason, 1996). Tabata et al. (Tabata and Aiyama, 2003) presented a passing manipulation. The trajectory of a 1-DOF manipulator was derived by Newton's method with top height of the parabolic orbit. Kato et al. (Kato and Nakamura, 1997) controlled releasing time of throwing. Pekarovskiy et al. (Pekarovskiy, Stockmann, Okada and Buss, 2014) developed a robust throwing algorithm which makes the robot follow the reference trajectory including impact reduction in catching. Arisumi et al. (Arisumi and Komoriya, 2002) developed a tension control method for trajectory modification of a thrown object.

On the other hand, because throwing is fast and dynamic, the motion will be finished before the controller produces its effects. Moreover, the robot system sometimes has zero adjustment error in the initial position on its joint angle. This error cannot be overcome by a robust controller, because it is not measured by sensors. Thus, we have proposed a robust trajectory design method so far (Okada, Pekarovskiy and Buss, 2015). In this method, dynamic sensitivity is considered. Figure 2 shows the concept of this method. In Fig. 2(a), the nominal initial position and release point A are represented

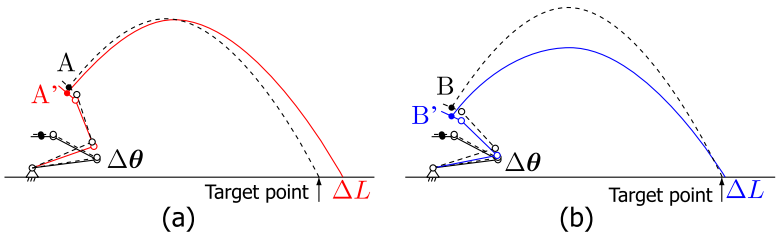

Fig. 2 Perturbation of landing point with respect to zero adjustment error

by dashed lines, and the object reaches to the target point. However, because of the zero adjustment error $\Delta\boldsymbol{\theta}$, the release point is changed to A' and the landing point has large perturbation which are represented by the solid lines. On the other hand, in Fig. 2(b), the release point is set to B. Same as Fig. 2(a), it is changed to B' because of $\Delta\boldsymbol{\theta}$. While the trajectory of the object is much different from the nominal one, the landing point is almost same as the target point. In this example, the throwing in Fig. 2(b) is more robust from 'accuracy of the landing' point of view. The sensitivity of the landing point with respect to the zero adjustment error is obtained by $E(\Delta L/\Delta\boldsymbol{\theta}) = \partial L/\partial\boldsymbol{\theta}$ where $E(\cdot)$ means expectation, and calculation method of $\partial L/\partial\boldsymbol{\theta}$ was developed in (Okada, Pekarovskiy and Buss, 2015) considering robot dynamics.

The main purpose of this paper is experimental evaluations of our conventionally proposed method, and motion design that enhances the accuracy of landing point. A three-link manipulator is prototyped and feed-forward/back controlled. The calculation method is developed for sensitivity of the landing point with respect to zero adjustment error, while the conventional method utilizes only feed-forward control. The effectiveness of the proposed method is evaluated based on the sensitivity and variance of the landing point, and a robust throwing with small sensitivity is designed.

2. Dynamic sensitivity analysis with feed-forward control

2.1. Sensitivity of landing point with respect to zero adjustment error

In this section, the conventional method of sensitivity analysis is explained. Sensitivity analysis has been often utilized for error assessment, optimal design of closed kinematic chain and control (Salisbury and Craig, 1982 and Cardou, Bouchard and Gosselin, 2010). Zhao-cai et al. introduced sensitivity for dynamics characteristic based on natural frequency of a flexible parallel robot (Zhao-cai, Yue-qing and Li-ying, 2006). Based on the relationship between output $\boldsymbol{y}$ and input parameter $\boldsymbol{x}$,

$$\boldsymbol{y} = \boldsymbol{f}(\boldsymbol{x}) \tag{1}$$

the sensitivity ${}^{y}S_{x}$ of $\boldsymbol{y}$ with respect to $\boldsymbol{x}$ is defined by:

$${}^{y}S_{x} = \frac{\partial \boldsymbol{f}}{\partial \boldsymbol{x}} \tag{2}$$

Because Eq. (1) is equality, these results would be regarded as 'static sensitivity' even though the output is natural frequency. On the other hand, we have proposed 'dynamic sensitivity' analysis (Okada, Pekarovskiy and Buss, 2015). In the followings of this section, the conventionally proposed method is illustrated.

Consider a three-link manipulator shown in Fig. 3. The robot starts from (a) initial position with its joint angle $\boldsymbol{\theta}_0$. $\boldsymbol{x}_0$ and ϕ_0 mean the initial value of the position $\boldsymbol{x}$ and orientation ϕ of the end-effector, respectively. $\dot{\boldsymbol{x}}_0 = \ddot{\boldsymbol{x}}_0 = 0$,

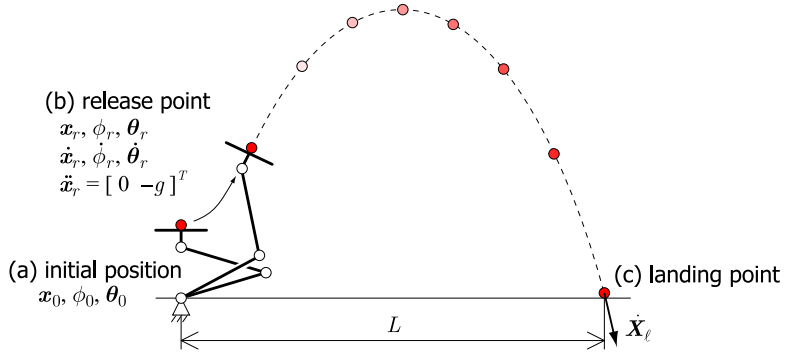

Fig. 3 Throwing motion of planner three-link manipulator

$\dot{\phi}_0 = \ddot{\phi}_0 = 0$ and $\dot{\boldsymbol{\theta}}_0 = \ddot{\boldsymbol{\theta}}_0 = 0$ are assumed. This robot throws an object (point mass m) so that it lands at the landing point L with feed-forward control. By setting the velocity $\dot{\boldsymbol{X}}_\ell$ of the object at (c) landing point, the trajectory of m is uniquely defined by a parabolic line. The (b) release point $\boldsymbol{x}_r$ is arbitrary selected on the parabolic line inside the workspace of the manipulator. $\dot{\boldsymbol{x}}_r$ is appropriately defined along the parabolic line, and $\ddot{\boldsymbol{x}}_r = [\ \ddot{x}_r \quad \ddot{y}_r\ ]^T$ should be $[\ 0 \quad -g\ ]^T$.

There are two types of uncertainties on the initial position of the manipulator. One is initial positioning error of the end-effector, the other is zero adjustment error of joint angles. The former will be overcome by position control, however, the latter cannot be because many robots use incremental position sensors (encoders). A positioning jig or sensor will be utilized for zero adjustment, however, because of elasticity of the jig or reaction region of the sensor, the joint angles would have uncertainties, which causes bias term of the joint angles. We have discussed about the positioning error in (Jin and Okada, 2015) and shown that there were some errors even though a jig was utilized. The focus of the sensitivity analysis in this research is sensitivity of landing point error ΔL with respect to zero adjustment error $\Delta\boldsymbol{\theta}_0$, which is represented by:

$$ {}^{L}S_{\boldsymbol{\theta}_0} = E\left(\frac{\Delta L}{\Delta\boldsymbol{\theta}_0}\right) = \frac{\partial L}{\partial\boldsymbol{\theta}_0} \tag{3} $$

2.2. Sensitivity analysis of L with respect to $\boldsymbol{\theta}_0$

Equation (3) is divided into three steps, which are (i) sensitivity of $\Delta\boldsymbol{\theta}_r$ and $\Delta\dot{\boldsymbol{\theta}}_r$ with respect to $\Delta\boldsymbol{\theta}_0$ ($= {}^{\boldsymbol{\theta}_r}S_{\boldsymbol{\theta}_0}$), (ii) sensitivity of $\Delta\boldsymbol{x}_r$, $\Delta\phi_r$, $\Delta\dot{\boldsymbol{x}}_r$ and $\Delta\dot{\phi}_r$ with respect to $\Delta\boldsymbol{\theta}_r$ and $\Delta\dot{\boldsymbol{\theta}}_r$ ($= {}^{\boldsymbol{X}_r}S_{\boldsymbol{\theta}_r}$), (iii) sensitivity of L with respect to $\Delta\boldsymbol{x}_r$, $\Delta\phi_r$, $\Delta\dot{\boldsymbol{x}}_r$ and $\Delta\dot{\phi}_r$ ($= {}^{L}S_{\boldsymbol{X}_r}$). By the definition of these parameters, Eq. (3) is written by:

$$ {}^{L}S_{\boldsymbol{\theta}_0} = \begin{bmatrix} \dfrac{\partial L}{\partial \boldsymbol{X}_r} & \dfrac{\partial L}{\partial \dot{\boldsymbol{X}}_r} \end{bmatrix} \begin{bmatrix} \dfrac{\partial \boldsymbol{X}_r}{\partial \boldsymbol{\theta}_r} & \dfrac{\partial \boldsymbol{X}_r}{\partial \dot{\boldsymbol{\theta}}_r} \\ \dfrac{\partial \dot{\boldsymbol{X}}_r}{\partial \boldsymbol{\theta}_r} & \dfrac{\partial \dot{\boldsymbol{X}}_r}{\partial \dot{\boldsymbol{\theta}}_r} \end{bmatrix} \begin{bmatrix} \dfrac{\partial \boldsymbol{\theta}_r}{\partial \boldsymbol{\theta}_0} \\ \dfrac{\partial \dot{\boldsymbol{\theta}}_r}{\partial \boldsymbol{\theta}_0} \end{bmatrix} = {}^{L}S_{\boldsymbol{X}_r}\,{}^{\boldsymbol{X}_r}S_{\boldsymbol{\theta}_r}\,{}^{\boldsymbol{\theta}_r}S_{\boldsymbol{\theta}_0} \tag{4} $$

$$ \boldsymbol{X}_r = \begin{bmatrix} \boldsymbol{x}_r^T & \phi_r \end{bmatrix}^T \tag{5} $$

2.2.1. Calculation of ${}^{L}S_{\boldsymbol{X}_r}$ Assuming small air friction, the object released at $\boldsymbol{x}_r$ with $\dot{\boldsymbol{X}}_r$ draws a parabolic line represented by;

$$ y = ax^2 + bx + c \tag{6} $$

where the coefficients a, b and c are obtained by;

$$ \boldsymbol{a} = \begin{bmatrix} a \\ b \\ c \end{bmatrix} = X^{-1}Y, \quad X = \begin{bmatrix} x_r^2 & x_r & 1 \\ 2x_r\dot{x}_r & \dot{x}_r & 0 \\ 2\dot{x}_r^2 & 0 & 0 \end{bmatrix}, \quad Y = \begin{bmatrix} y_r \\ \dot{y}_r \\ -g \end{bmatrix} \tag{7} $$

and L is obtained by;

$$ L = \frac{-b - \sqrt{b^2 - 4ac}}{2a} \quad (a < 0) \tag{8} $$

as the solution of $y = 0$ in Eq. (6). From Eqs. (7) and (8), ${}^{L}S_{\boldsymbol{X}_r}$ is obtained by;

$$ {}^{L}S_{\boldsymbol{X}_r} = \begin{bmatrix} \dfrac{\partial L}{\partial \boldsymbol{a}}\dfrac{\partial \boldsymbol{a}}{\partial \boldsymbol{X}_r} & \dfrac{\partial L}{\partial \boldsymbol{a}}\dfrac{\partial \boldsymbol{a}}{\partial \dot{\boldsymbol{X}}_r} \end{bmatrix} \in R^{1\times 6} \tag{9} $$

$$\frac{\partial L}{\partial \boldsymbol{a}} = \left[\begin{array}{ccc} \dfrac{b^2 - 2ac + bD}{2a^2 D} & -\dfrac{b+D}{2aD} & \dfrac{1}{D} \end{array} \right], \quad D = \sqrt{b^2 - 4ac} \tag{10}$$

$$\frac{\partial \boldsymbol{a}}{\partial \boldsymbol{X}_r} = \left[\begin{array}{ccc} \dfrac{\partial X^{-1}}{\partial x_r} Y & \dfrac{\partial X^{-1}}{\partial y_r} Y & \dfrac{\partial X^{-1}}{\partial \phi_r} Y \end{array} \right] + X^{-1} \frac{\partial Y}{\partial \boldsymbol{X}_r} \tag{11}$$

$$\frac{\partial \boldsymbol{a}}{\partial \dot{\boldsymbol{X}}_r} = \left[\begin{array}{ccc} \dfrac{\partial X^{-1}}{\partial \dot{x}_r} Y & \dfrac{\partial X^{-1}}{\partial \dot{y}_r} Y & \dfrac{\partial X^{-1}}{\partial \dot{\phi}_r} Y \end{array} \right] + X^{-1} \frac{\partial Y}{\partial \dot{\boldsymbol{X}}_r} \tag{12}$$

where the relation of

$$\frac{\partial A^{-1}}{\partial x} = -A^{-1} \frac{\partial A}{\partial x} A^{-1} \tag{13}$$

will be utilized for calculation.

2.2.2. Calculation of ${}^{X_r}\boldsymbol{S}_{\theta_r}$ ${}^{X_r}S_{\theta_r}$ is obtained form kinematic relationship between joint angle and position / orientation of the end-effector. Assume that the kinematic relationship is represented by;

$$\boldsymbol{X}_r = \boldsymbol{F}(\boldsymbol{\theta}_r), \quad \boldsymbol{\theta}_r = \left[\begin{array}{ccc} \theta_{1r} & \theta_{2r} & \theta_{3r} \end{array} \right]^T \tag{14}$$

where θ_1, θ_2 and θ_3 are each joint angles. From Eq. (14), it is easily obtained;

$$\dot{\boldsymbol{X}}_r = \frac{\partial \boldsymbol{F}(\boldsymbol{\theta}_r)}{\partial \boldsymbol{\theta}} \dot{\boldsymbol{\theta}}_r \tag{15}$$

and ${}^{X_r}S_{\theta_r}$ is calculated by;

$${}^{X_r}S_{\theta_r} = \left[\begin{array}{cc} \dfrac{\partial \boldsymbol{F}(\boldsymbol{\theta}_r)}{\partial \boldsymbol{\theta}} & 0 \\ \dfrac{\partial^2 \boldsymbol{F}(\boldsymbol{\theta}_r)}{\partial \boldsymbol{\theta}^2} \dot{\boldsymbol{\theta}}_r & \dfrac{\partial \boldsymbol{F}(\boldsymbol{\theta}_r)}{\partial \boldsymbol{\theta}} \end{array} \right] \in R^{6\times 6} \tag{16}$$

$$\frac{\partial^2 \boldsymbol{F}(\boldsymbol{\theta}_r)}{\partial \boldsymbol{\theta}^2} \dot{\boldsymbol{\theta}}_r = \left[\begin{array}{ccc} \dfrac{\partial}{\partial \theta_1} \left(\dfrac{\partial \boldsymbol{F}(\boldsymbol{\theta}_r)}{\partial \boldsymbol{\theta}} \right) \dot{\boldsymbol{\theta}}_r & \dfrac{\partial}{\partial \theta_2} \left(\dfrac{\partial \boldsymbol{F}(\boldsymbol{\theta}_r)}{\partial \boldsymbol{\theta}} \right) \dot{\boldsymbol{\theta}}_r & \dfrac{\partial}{\partial \theta_3} \left(\dfrac{\partial \boldsymbol{F}(\boldsymbol{\theta}_r)}{\partial \boldsymbol{\theta}} \right) \dot{\boldsymbol{\theta}}_r \end{array} \right] \in R^{3\times 3} \tag{17}$$

where

$$\frac{\partial \boldsymbol{F}(\boldsymbol{\theta}_r)}{\partial \boldsymbol{\theta}} = \left. \frac{\partial \boldsymbol{F}(\boldsymbol{\theta})}{\partial \boldsymbol{\theta}} \right|_{\boldsymbol{\theta}=\boldsymbol{\theta}_r} \in R^{3\times 3} \tag{18}$$

is defined.

2.2.3. Calculation of ${}^{\theta_r}\boldsymbol{S}_{\theta_0}$ and ${}^{L}\boldsymbol{S}_{\theta_0}$ Assume that the dynamic equation of the robot is represented by the following state-space formulation,

$$\dot{\boldsymbol{q}} = \boldsymbol{f}(\boldsymbol{q}) + \boldsymbol{g}(\boldsymbol{q})\boldsymbol{\tau}, \quad \boldsymbol{q} = \left[\begin{array}{cc} \boldsymbol{\theta}^T & \dot{\boldsymbol{\theta}}^T \end{array} \right]^T, \quad \boldsymbol{\tau} = \left[\begin{array}{ccc} \tau_1 & \tau_2 & \tau_3 \end{array} \right]^T \tag{19}$$

where τ_i means joint torque. By time integrating of Eq. (19) with convolution integral, the closed form solution $\boldsymbol{q}_r$ is obtained. However, because Eq. (19) includes highly nonlinear functions, $\boldsymbol{q}_r$ is difficult to be calculated. Thus, we consider a time sequence data of trajectory for throwing as;

$$Q = \left\{ \begin{array}{cccc} \boldsymbol{q}_0 & \boldsymbol{q}_1 & \cdots & \boldsymbol{q}_r \end{array} \right\}, \quad T = \left\{ \begin{array}{cccc} \boldsymbol{\tau}_0 & \boldsymbol{\tau}_1 & \cdots & \boldsymbol{\tau}_r \end{array} \right\} \tag{20}$$

and Eq. (19) is linearized around each point as;

$$\dot{\boldsymbol{q}}_k = A_k^c \boldsymbol{q}_k + B_k^c \boldsymbol{\tau}_k + C_k^c \tag{21}$$

$$A_k^c = \frac{\partial \boldsymbol{f}(\boldsymbol{q}_k)}{\partial \boldsymbol{q}} + \left[\begin{array}{ccc} \dfrac{\partial \boldsymbol{g}(\boldsymbol{q}_k)}{\partial \theta_1} \boldsymbol{\tau}_k & \cdots & \dfrac{\partial \boldsymbol{g}(\boldsymbol{q}_i)}{\partial \dot{\theta}_3} \boldsymbol{\tau}_k \end{array} \right], \quad B_k^c = \boldsymbol{g}(\boldsymbol{q}_k), \quad C_k^c = \boldsymbol{f}(\boldsymbol{q}_k) - A_k^c \boldsymbol{q}_k \tag{22}$$

and discretized using trapezoidal integration (Tustin transformation) as:

$$\boldsymbol{q}_{k+1} = A_k \boldsymbol{q}_k + B_k^1 \boldsymbol{\tau}_k + B_k^2 \boldsymbol{\tau}_{k+1} + C_k \tag{23}$$

$$A_k = \left(I - \frac{\Delta t}{2} A_{k+1}^c \right)^{-1} \left(I + \frac{\Delta t}{2} A_k^c \right), \quad B_k^1 = \left(I - \frac{\Delta t}{2} A_{k+1}^c \right)^{-1} \frac{\Delta t}{2} B_k^c \tag{24}$$

$$B_k^2 = \left(I - \frac{\Delta t}{2} A_{k+1}^c \right)^{-1} \frac{\Delta t}{2} B_{k+1}^c, \quad C_k = \left(I - \frac{\Delta t}{2} A_{k+1}^c \right)^{-1} \frac{\Delta t}{2} (C_k^c + C_{k+1}^c) \tag{25}$$

where I is an identity, Δt is a sampling time. By the recursive calculation of Eq. (23), $\boldsymbol{q}_r$ is obtained by:

$$\boldsymbol{q}_r = \mathcal{A}\boldsymbol{q}_0 + \mathcal{B}\begin{bmatrix} \boldsymbol{\tau}_0 \\ \vdots \\ \boldsymbol{\tau}_r \end{bmatrix} + C \tag{26}$$

$$\mathcal{A} = \prod_{k=1}^{r-1} A_k \tag{27}$$

$$\mathcal{B} = \begin{bmatrix} \prod_{k=2}^{r-1} A_k B_1^1 & \left(\prod_{k=2}^{r-1} A_k B_1^2 + \prod_{k=3}^{r-1} A_k B_2^1\right) & \cdots & \left(A_{r-2}B_{r-2}^2 + B_{r-1}^1\right) & B_{r-1}^2 \end{bmatrix} \tag{28}$$

$$C = \prod_{k=2}^{r-1} A_k C_1 + \prod_{k=3}^{r-1} A_k C_2 + \cdots + C_{r-1} \tag{29}$$

Based on Eq. (26), ${}^{\theta_r}S_{\theta_0}$ is obtained by:

$${}^{\theta_r}S_{\theta_0} = \mathcal{A}\begin{bmatrix} I \\ 0 \end{bmatrix} \in R^{6\times 3} \tag{30}$$

By using Eqs. (9), (16) and (30), ${}^{L}S_{\theta_0}$ in Eq. (4) is obtained.

2.3. Sensitivity analysis and throwing simulation

Figure 4 shows the result of sensitivity analysis using the proposed method. The red dashed line shows a parabolic

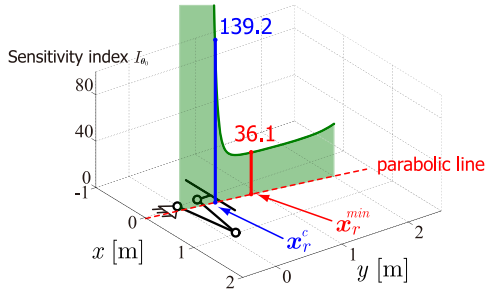

Fig. 4 Sensitivity of L with respect to the initial position

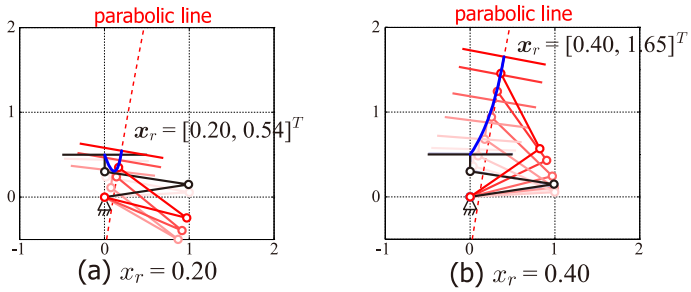

Fig. 5 Example of the throwing motion

locus of the object that passes through the reference landing point ($L = 5$). The release point $\boldsymbol{x}_r$ is selected on the parabolic line. The motion of the robot Q in Eq. (20) is defined by 5th order time function, where the coefficients are determined by boundary conditions of $\boldsymbol{\theta}_0$, $\dot{\boldsymbol{\theta}}_0$, $\ddot{\boldsymbol{\theta}}_0$ and $\boldsymbol{\theta}_r$, $\dot{\boldsymbol{\theta}}_r$, $\ddot{\boldsymbol{\theta}}_r$. T is calculated by inverse dynamic computation. Figure 5 shows examples of the throwing motion when $x_r = 0.2$ and 0.4. The red dashed line shows a parabolic line (same as in Fig. 4), the black line shows the initial posture, blue line shows the trajectory of the end effector and red postures show time sequence postures of the throwing robot. Because ${}^{L}S_{\theta_0}$ is defined by $R^{1\times 3}$ vector, the sensitivity index $I_{\boldsymbol{\theta}_0}$

$$I_{\boldsymbol{\theta}_0} = \left\| {}^{L}S_{\theta_0} \right\| \tag{31}$$

is introduced. By selecting $\boldsymbol{x}_r = \boldsymbol{x}_r^{min} = [\ 0.246\ \ 0.912\ ]^T$, $I_{\boldsymbol{\theta}_0}$ is minimized, which is represented by red point in Fig. 4. To show the effectiveness of the sensitivity analysis, throwing simulations are executed. By changing the initial position of the manipulator, the distribution of L are calculated. The initial joint angles are set by;

$$\boldsymbol{\theta}(0) = \boldsymbol{\theta}_0 + N(0, \sigma^2) \tag{32}$$

where $\boldsymbol{\theta}_0$ is a nominal value and $N(0, \sigma^2)$ means Gaussian perturbation with zero mean and σ^2 variance. Monte-Carlo simulations are executed 2000 times. For comparison, another $\boldsymbol{x}_r = \boldsymbol{x}_r^c$ with larger sensitivity is selected with $\boldsymbol{x}_r^c = [\ 0.180\ \ 0.431\ ]^T$, which is indicated by blue point in Fig. 4. In these simulations, Runge-Kutta integral is utilized for forward dynamics computation. Figure 6 shows the loci of the object in the simulation, and Fig. 7 shows a histogram of the landing point. By selecting $\boldsymbol{x}_r = \boldsymbol{x}_r^{min}$, the variance of the landing point is much smaller than $\boldsymbol{x}_r = \boldsymbol{x}_r^c$. Moreover, the ratio of $I_{\boldsymbol{\theta}_0}$ and a square root of the variance (standard deviation) in each motion are almost same as:

$$\frac{36.1}{139.2} = 0.259 \simeq \frac{\sqrt{0.030}}{\sqrt{0.474}} = 0.252 \tag{33}$$

These results show that the sensitivity calculation by the proposed method well represents the value of the variance on the landing point.

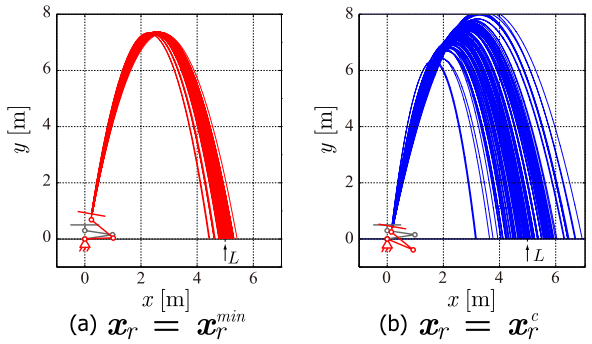

Fig. 6 Loci of flying object with perturbations of the initial joint angle

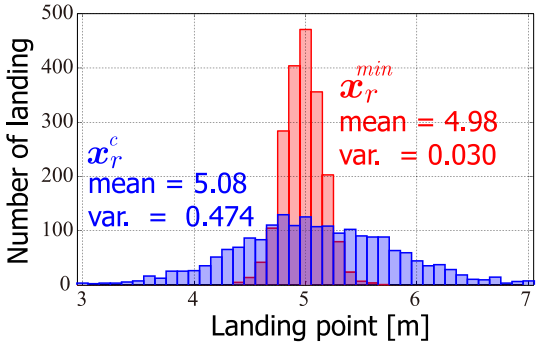

Fig. 7 Histogram of the landing point

3. Experimental evaluation of sensitivity analysis

3.1. Experimental system

To evaluate the effectiveness of the proposed method, a three-link manipulator is prototyped. Figure 8 shows the prototyped three-link manipulator and configurations of the throwing. 60W DC-motor (Maxon Co.) and a reduction gear

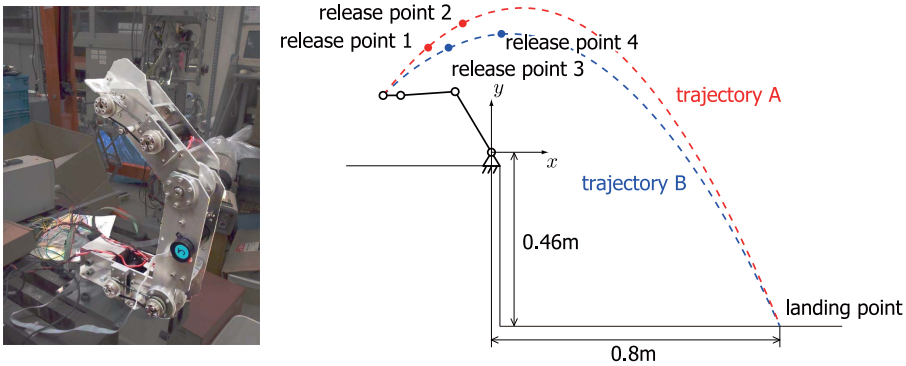

Fig. 8 Prototype of the three-link manipulator and throwing configuration

(reduction ratio: 50, Harmonic Drive Systems Inc.) are utilized on each joint. The manipulator has almost same size as human arm, and fixed on the table with its height = 0.46 m. The landing point is selected on the floor with its distance = 0.8 m. By selecting two $\dot{X}_\ell$ (velocity of the object at landing point), trajectory A and B are defined. And four release point 1~4 are set. The initial position θ_0 of the manipulator is adjusted by using a jig in every experiments, and known small error of the joints are added. The sampling time of control is 100 μsec utilizing a Windows 7 desktop computer.

3.2. Sensitivity analysis with feed-forward/back control

Because there are so many physical uncertainties on the experimental system and for safety issue, both feed-forward and feed-back control (with PD controller) are introduced for experiments. The state-space representation of the dynamics in Eq. (21) is changed by;

$$\dot{q}_k = \left(A_k^c - B_k^c \begin{bmatrix} K_p & K_d \end{bmatrix}\right) q_k + B_k^c \tau_k + \left(C_k^c + B_k^c \begin{bmatrix} K_p & 0 \end{bmatrix} q_k^{ref}\right) \tag{34}$$

where K_p and K_d are feed-back gain that yields the feed-back torque;

$$\tau_k^b = \begin{bmatrix} K_p & K_d \end{bmatrix} \begin{bmatrix} \theta_k^{ref} - \theta_k \\ -\dot{\theta}_k \end{bmatrix} \tag{35}$$

where θ_k^{ref} is a reference joint angle of throwing. Moreover, because of the high gain feed-back, the joint error $\Delta\theta_0$ remains as a bias term of θ^{ref} as shown in Fig. 9, which is equivalent to shifting of θ^{ref} to $\theta^{ref} + \Delta\theta_0$. Because Q in Eq. (20) ($= q^{ref}$) and A_k^c, C_k^c in Eq. (21) are functions of θ^{ref} then $\mathcal{A}$, $\mathcal{B}$ and C in Eq. (26) are functions of $\Delta\theta_0$. From these considerations, the sensitivity ${}^{\theta_r}S_{\theta_0}$ in Eq. (30) is changed by:

$${}^{\theta_r}S_{\theta_0} = \mathcal{A} \begin{bmatrix} I \\ 0 \end{bmatrix} + \frac{\partial \mathcal{A}}{\partial Q}\frac{\partial Q}{\partial \theta_0} + \frac{\partial \mathcal{B}}{\partial Q}\frac{\partial Q}{\partial \theta_0} \begin{bmatrix} \tau_0 \\ \vdots \\ \tau_r \end{bmatrix} + \frac{\partial C}{\partial Q}\frac{\partial Q}{\partial \theta_0} \tag{36}$$

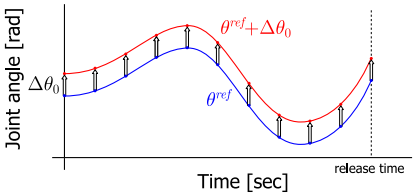

Fig. 9 Influence of the inital joint error to the trajectory

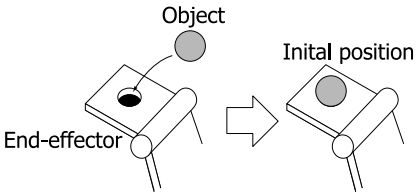

Fig. 10 Putting an object on the end-effector

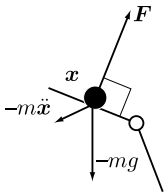

Fig. 11 Orientation of the end-effector

In this paper, $\partial\mathcal{A}/\partial Q$, $\partial\mathcal{B}/\partial Q$ and $\partial\mathcal{C}/\partial Q$ are calculated by numerical computation for simplicity. Note that $\boldsymbol{\tau}_0$, $\boldsymbol{\tau}_1$ $\cdots$ are constant values because they are yielded by feed-forward control.

3.3. Sensitivity analysis of throwing

3.3.1. Design of throwing trajectory In section 2, it is assumed that the object is fixed on the end-effector through the throwing motion of the manipulator. On the other hand, in the experiment, even though the object (sphere iron ball) is put on the end-effector with a hole as shown in Fig.10, it is not fixed. So, the throwing trajectory is designed by 7th order polynomial of time function so that the direction of the reaction force to the object takes orthogonal direction to the end-effector as shown in Fig. 11. The boundary condition is obtained by:

$$\boldsymbol{x}(0) = \begin{bmatrix} x_0 & y_0 \end{bmatrix}^T, \qquad \dot{\boldsymbol{x}}(0) = 0, \qquad \ddot{\boldsymbol{x}}(0) = \boldsymbol{x}^{(3)}(0) = \boldsymbol{x}^{(4)}(0) = 0 \tag{37}$$

$$\boldsymbol{x}_r = \begin{bmatrix} x_r & y_r \end{bmatrix}^T, \qquad \dot{\boldsymbol{x}}_r = \begin{bmatrix} \dot{x}_r & \dot{y}_r \end{bmatrix}^T, \qquad \ddot{\boldsymbol{x}}_r = \begin{bmatrix} 0 & -g \end{bmatrix}^T \tag{38}$$

ϕ is automatically defined by the constraint of reaction force. $\boldsymbol{x}^{(4)}(0) = 0$ is for smooth change of the orientation of the end-effector. The joint trajectory of the throwing is obtained by inverse kinematic computation based on position $\boldsymbol{x}$ and orientation ϕ of the end-effector. Throwing motion at release point 1 is shown in Fig. 12 and snapshot of the experiment is shown in Fig. 13. The landing point is measured using carbon paper.

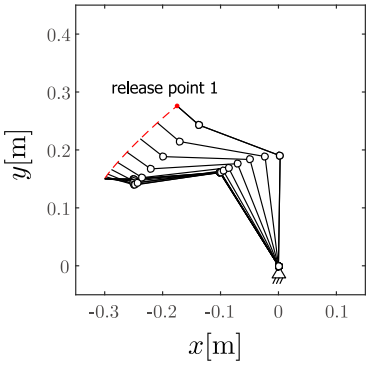

Fig. 12 Throwing motion at release point 1

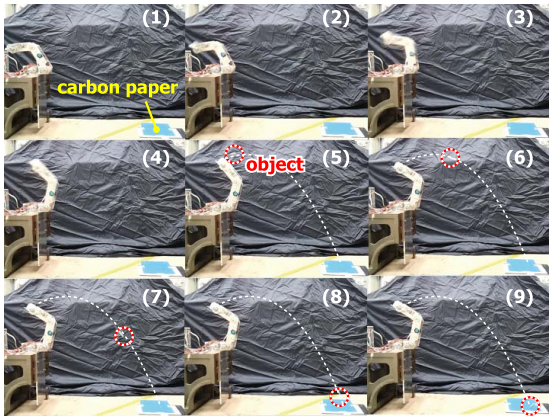

Fig. 13 Snapshot of experiments

3.3.2. Sensitivity analysis and experimental evaluation Based on the proposed method, the sensitivity analysis is executed. Figure 14 shows the results. $\boldsymbol{x}_r$ is selected along the parabolic line of trajectory A and B. I_{θ_0} in Eq. (31) is utilized. Because of the restriction of the motor torque and angular velocity, the throwing is impossible in the yellow area. The sensitivity on the release point 1~4 are indicated by the red line. By selecting $\boldsymbol{x}_r$ at the release point 4, the sensitivity is small.

The experiments are executed on release point 1~4, and the landing points are measured. The results are shown in Figs. 15 and 16. For the evaluation of the proposed method, two types of the experiments are executed. The first one is a normal experiment. The robot joint encoders are initialized by a jig, and throwing is executed 50 times, which is indicated by "without error". In the second experiment, after initialization of the joint angle with a jig, pre-determined error (zero adjustment error) is added with 1° variance white noise, which is indicated "with error". The experiments are executed 80 times. The upper figures show measured data of the landing, and the lower figures show histograms. Because there are so many uncertainties (model uncertainties, friction term, time delay of the motor driver (current control), and so on), even though there is not initial joint error ($N(0, \sigma^2) = 0$ in Eq. (32)), the landing point has distribution, which is shown in Figs.

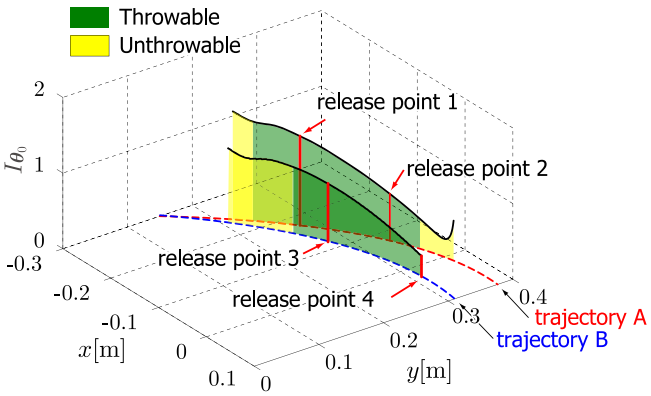

Fig. 14 Sensitivity analysis on the experimental system

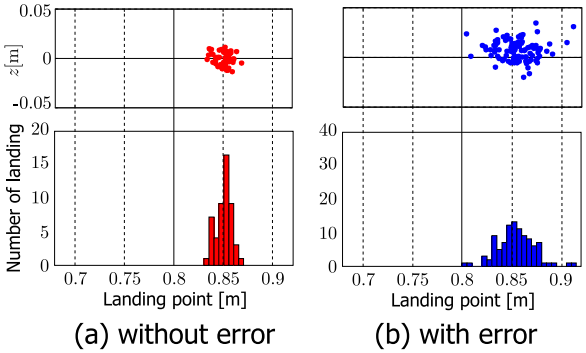

Fig. 15 Distribution of landing point (release point 1)

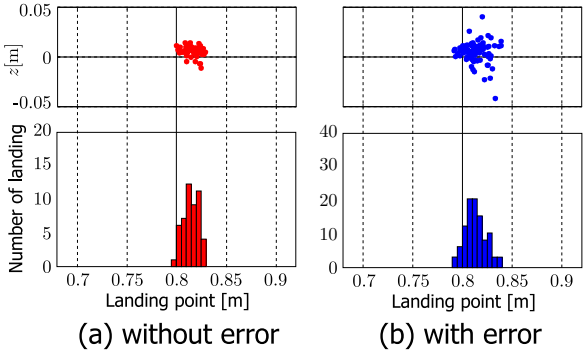

Fig. 16 Distribution of landing point (release point 4)

15(a) and 16(a). It can be considered that these distributions are caused by 'mechanical uncertainties'. On the other hand, the variance in Fig. 16(b) is smaller than Fig. 15(b), which corresponds to the smaller sensitivity of release point 4 than release point 1.

Table 1 shows the value of sensitivity and standard deviation of the measured data on each release point, where

Table 1 Experimental result of each release point

No. of release point	1	2	3	4
$\frac{\pi}{180} I_{\theta_0} \times 10^3$	19.2	10.2	12.6	4.69
SD_0[mm]	7.86	6.88	5.15	7.61
SD_e [mm]	18.4	14.9	15.6	10.2
SD_e^{est}[mm]	20.8	12.3	13.6	8.95

the dimension of I_{θ_0} is changed from m/rad to mm/rad using the variance of $\Delta\boldsymbol{\theta}_0$ is 1.0 deg^2 (which is utilized in the experiments). SD_0 and SD_e mean standard deviation of the distribution of landing point 'without error' and 'with error' respectively. Moreover, with the assumption that $\Delta\boldsymbol{\theta}_0$ is independent to the mechanical error, SD_e is estimated by;

$$SD_e^{est} = \sqrt{(SD_0)^2 + \left(\frac{\pi}{180} I_{\theta_0} \times 10^3\right)^2} \tag{39}$$

which is also shown in Table 1. The effectiveness of the sensitivity analysis is evaluated by similarity of SD_e and SD_e^{est}. Figure 17 shows the relationship between SD_e and SD_e^{est} on each release point. The error bar represents 99% confident interval of the population standard deviation (Note that the upper bar is longer). Because the error bars of SD_e and SD_e^{est} have common area, the sensitivity obtained by the proposed method well represents the distribution of the landing point, which shows the effectiveness of the proposed method.

3.4. Robust throwing design based on sensitivity analysis

In all throwable area, the sensitivity is calculated based on the proposed method. The results are shown in Fig. 18. The sensitivity takes minimum value $\frac{\pi}{180} I_{\theta_0} \times 10^3 = 1.30$ at $\boldsymbol{x}_r = \boldsymbol{x}_r^{min}$, which is much smaller than that of release point

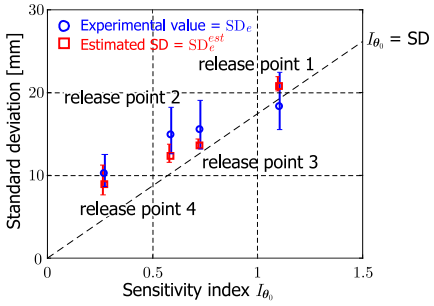

Fig. 17 Relationship between SD_e and SD_e^{est}

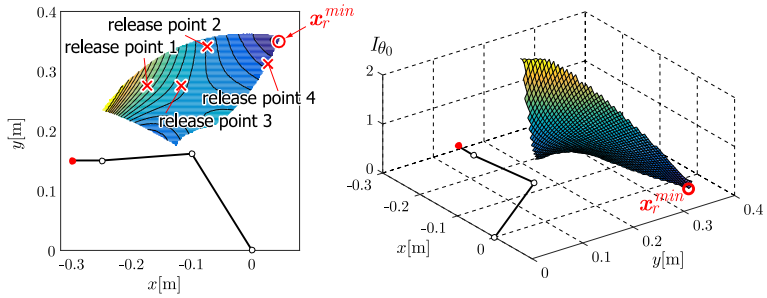

Fig. 18 Sensitivity analysis in throwable area

1~4 (refer to Table 1). The throwing motion at $\boldsymbol{x}_r = \boldsymbol{x}_r^{min}$ and experimental results (histogram of the landing) are shown in Fig. 19 and Fig. 20 respectively. From the results of Fig. 20, $SD_0 = 8.15$, $SD_e = 8.75$ are obtained. Because $SD_0 \simeq$

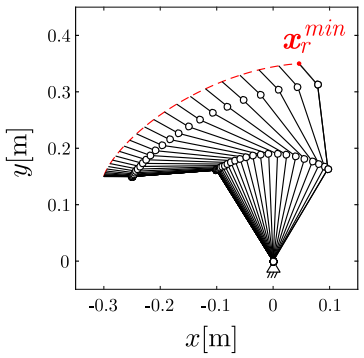

Fig. 19 Throwing motion at $\boldsymbol{x}_r = \boldsymbol{x}_r^{min}$

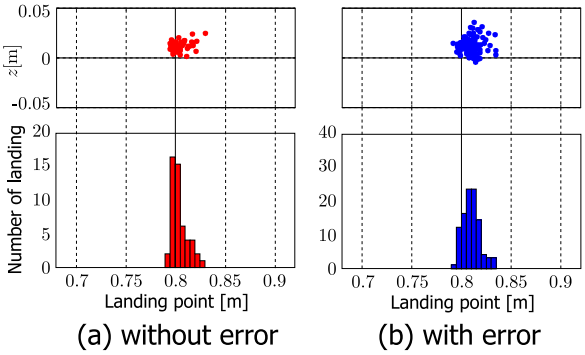

Fig. 20 Distribution of landing point ($\boldsymbol{x}_r = \boldsymbol{x}_r^{min}$)

SD_e is satisfied, the influence of $\Delta\boldsymbol{\theta}_0$ to landing distribution is highly reduced, which coincides to small I_{θ_0}.

The following is one example of probability of goal. Consider that the object is a ball with its diameter 20 mm which

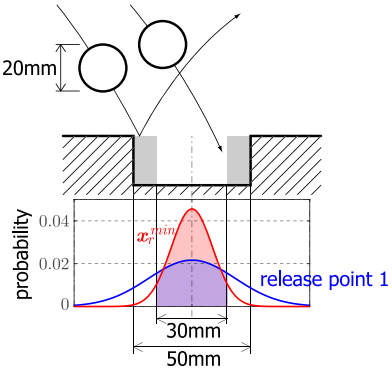

Fig. 21 Landing distribution

is utilized in this experiment, and there is a hole with its diameter 50 mm at the landing point (same size of a coffee can) as shown in Fig.21. The probability of goal is 58.6% using release point 1 while 91.4% using $\boldsymbol{x}_r^{min}$, which is obtained by integral of Gaussian function of $N(0, SD_e^2)$.

4. Conclusions

In this paper, we have proposed dynamics sensitivity analysis method focusing on a throwing by a powered manipulator. The sensitivity of the landing point with respect to zero adjustment error of the joints has been introduced, and robust throwing that has small sensitivity has been designed. The effectiveness of the proposed method has been evaluated by simulations and experiments. The results are summarized as follows;

(1) By setting a trajectory of throwing, the dynamics of the manipulator is linearized and discretized along the trajectory, which enables the closed form solution of forward dynamic analysis.

(2) Based on the obtained closed form solution, the sensitivity analysis is executed for the landing point with respect to joint zero adjustment error.

(3) Sensitivity analysis for feed-forward/back controlled manipulator is introduced.

(4) A planner three-link manipulator is prototyped, and the effectiveness of the proposed method is evaluated based on error analysis from stochastic point of view.

(5) Based on the proposed method, the robust motion that yields high probability of goal for throwing is designed.

Acknowledgment

This research is supported by JSPS Grants-in-Aid for Scientific Research (Category: Scientific Research C) entitled 'Motion optimization and instruction of throwing based on sensitivity analysis with respect to uncertainties'.

References

Arisumi, H. and Komoriya, K., Casting Manipulation (3rd Report, Analysis on Viscoelasticity of Flexible String and Mid-Air Trajectory Control of Gripper by Impulse Force), Transactions of the Japan Society of Mechanical Engineering Series C, Vol.68, No.665, (2002), pp.139 – 146 (in Japanese).

Cardou, P., Bouchard, S. and Gosselin, C., Kinematic-Sensitivity Indices for Dimensionally Nonhomogeneous Jacobian Matrices, IEEE Transactions on Robotics, (2010), Vol. 26, No. 1, pp.166–173.

Fagiolini, A., Arisumi, H. and Bicchi, A., Casting robotic end-effectors to reach faraway moving objects, Computing Research Repository (CoRR), Vol. abs/1101.2268, (2011).

Frank, H., Barteit, D. and Kupzog, F., Throwing or shooting - a new technology for logistic chains within production system, Proc. of the IEEE International Conference on Technologies for Practical Robot Applications (TePRA 2008), (2008), pp.62 – 67.

Jin, J. H. and Okada, M., Human-error Analysis for Robust Trajectory Design, Proc. of 2015 JSME Conference on Robotics and Mechatronics (Robomec2015), (2015), 2P1-N06 (in Japanese).

Kato, N. and Nakamura, T., Throwing Control for 2-DOF Robot (Adaptive Control and Online Modification of Release Time), Transactions of the Japan Society of Mechanical Engineering Series C, Vol.63, No.614, (1997), pp.3571 – 3576 (in Japanese).

Lynch, K. M. and Mason, M. T., Dynamic underacutated nonprehensile manipulation, Proc. of the IEEE/RSJ International Conference on Intelligent Robots and Systems (IROS1996), (1996), pp.889 – 896.

Mason, M. T. and Lynch, K. M., Dynamic manipulation, Proc. of the IEEE/RSJ International Conference on Intelligent Robots and Systems (IROS1993), (1993), pp.152 – 159.

Okada, M., Pekarovskiy, A. and Buss, M., Robust Trajectory Design for Object Throwing based on Sensitivity for Model Uncertainties, Proc. of the IEEE International Conference on Robotics and Automation (ICRA2015), (2015), pp.3089 – 3094.

Pekarovskiy, A., Stockmann, F., Okada, M. and Buss, M. Hierarchical Robustness Approach for Nonprehensile Catching of Rigid Objects, Proc. of the IEEE/RSJ International Conference on Intelligent Robots and Systems (IROS2014), (2014), pp.3649–3654.

Salisbury, J. K. and Craig, J. J., Articulated Hands: Force Control and Kinematic Issues, The International Journal of Robotics Research, (1982), Vol. 1, No. 1, pp. 4–17.

Tabata, T. and Aiyama, Y., Passing manipulation by 1 degree-of-freedom manipulator - catching manipulation of tossed object without impact, Proc. of the IEEE/RSJ International Conference on Intelligent Robots and Systems (IROS2003), Vol.3, (2003), pp.2920 – 2925.

Tsukakoshi, H., Watari, E., Fuchigami, K., and Kitagawa, A., Casting device for search and rescue aiming higher and faster access in disaster site, Proc. of the IIEEE/RSJ International Conference on Intelligent Robots and Systems (IROS'12), (2012), pp.4348 – 4353.

Zhao-cai, D., Yue-qing, Y. and Li-ying, S., Sensitivity Analysis for Dynamic Characteristic of Flexible Parallel Robots, Proc. of the 2006 IEEE International Conference on Robotics and Biomimetics, (2006), pp.1151–1156.